

H. GARBACZ*, P. WIECIŃSKI*, T. WIERZCHOŃ*, K. J. KURZYDŁOWSKI*

EFFECT OF SURFACE TREATMENT ON THE MICROSTRUCTURE OF TA6V

WPLYW OBRÓBKI POWIERZCHNIOWEJ NA MIKROSTRUKTURĘ STOPU TA6V

Methods of surface engineering are used to improve microhardness and wear resistance of Ti alloys. Magnetron sputtering or vacuum evaporation processes combined with annealing under glow discharge conditions were used to obtain Ti-Al intermetallic layers on the surface of TA6V alloy. The layers have diffusional character and contain Ti_3Al + $TiAl$ + $TiAl_3$ + Al_2O_3 phases. The microstructures of the TA6V subjected to each treatment alone differ profoundly from the one obtained in combination of these methods.

Metody inżynierii powierzchni znalazły zastosowanie do poprawy mikrotwardości i odporności na ścieranie stopów tytanu. W niniejszej pracy zastosowano kombinację technik PVD (naparowywanie próżniowe lub rozpylanie magnetronowe) i CVD (wyżarzanie w warunkach wyładowania jarzeniowego). W wyniku przeprowadzonych obróbek, na materiale podłoża, otrzymano kompozytowe warstwy międzymetaliczne z układu Ti-Al o charakterze dyfuzyjnym i następującym składzie fazowym: Ti_3Al + $TiAl$ + $TiAl_3$ + Al_2O_3 . Mikrostruktura stopu TA6V oraz warstw międzymetalicznych otrzymanych w wyniku zastosowania pojedynczych obróbek powierzchni znacznie różni się od otrzymanej w wyniku kombinacji tych metod. Najbardziej optymalną warstwę międzymetaliczną przy jednoczesnym zachowaniu mikrostruktury podłoża uzyskano w wyniku połączenia rozpylania magnetronowego z obróbką jarzeniową.

1. Introduction

Titanium alloys are lightweight materials with high fatigue, creep and good corrosion resistance. However, applications of titanium and its alloys are limited by their relatively low hardness and poor tribological properties. Thus, the elements made of titanium alloy, widely used in aerospace and automotive industries are frequently coated by CVD, PVD, plasma spraying, or diffusion layers [1–4]. In the present study hybrid treatments have been used to change surface phase composition of TA6V alloy [5–8]. The treatments consisted of two stages. First, the titanium alloy was covered with aluminum layer either by vacuum evaporation or magnetron sputtering. In the second stage, coated specimens were treated under glow discharge conditions. The paper also reports the results of studies of the microstructure of TiAl6V samples obtained in the above mentioned treatments applied in combination and separately.

2. Experimental details

The material used was a TA6V titanium alloy (wt%: 6,4Al, 4,1V, 0,1C, 0,16Fe, 0,18O, 0,01N, 0,003H, balance Ti) delivered in the form of rolled bars 12mm in diameter. The samples cut from the bars prior to coating were 3 mm thick discs. The aluminum layer was formed on the titanium alloy substrate using either vacuum evaporation or magnetron sputtering. The aluminum coated samples were annealed: (a) under glow discharge conditions at 700°C in an argon and (b) under vacuum of 10^{-3} hPa at 500°C, 600°C, 700°C. Both glow discharge and no glow discharge annealings were carried out for 2h.

The investigations reported here focused on phase transformations occurring as a result of the surface treatments. The microstructure of surface layers were examined using a light and scanning electron microscope with Energy Dispersive Spectrometer (EDS). Volume frac-

* FACULTY OF MATERIALS SCIENCE AND ENGINEERING, WARSAW UNIVERSITY OF TECHNOLOGY, 02-507 WARSAW, 141 WOŁOSKA STR., POLAND

tions of different phases were determined by stereological method and XRD analyses.

3. Results

Phases transitions in the TA6V-Al couple

Fig. 1. shows XRD diffraction patterns of the TA6V samples coated with aluminum after annealing at 500°C, 600°C, 700°C under vacuum of 10^{-3} hPa. After annealing at 500°C only diffraction lines of titanium and aluminum were observed. There was no diffraction peaks of intermetallic phases of Ti-Al system, despite the fact that diffusion in the titanium – aluminum couple is already quite fast even in lower temperatures as showed by Peng et al [9]. It was also found that the diffusion of the titanium in aluminum proceeds faster in Al(110) crystallographic directions than in (100) and (111) planes. In this study the TA6V titanium alloy was used as substrate, which contains 6% aluminum and 4% vanadium. As a results, the chemical gradient of the aluminum is smaller in TA6V-Al than in Ti-Al system. The smaller chemical gradient can decrease the diffusion rate and no intermetallic phases were formed due to annealing at 500°C. On the other hand, in the XRD diffraction patterns a shift in the diffraction lines of aluminum was observed. This indicates changes in lattice parameter of aluminum caused by diffusion of titanium and aluminum at the interface due to the different size of the Ti and Al atoms [9].

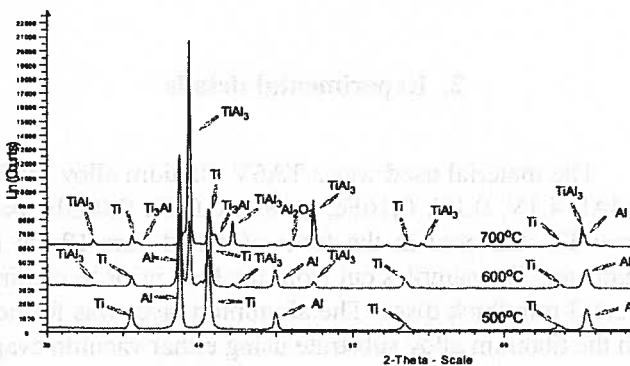


Fig. 1. The XRD diffraction patterns of the samples after annealing at 500°C, 600°C, 700°C

The X-ray diffraction patterns of the sample annealed at 600°C show the presence of the titanium, aluminum and $TiAl_3$ intermetallic phase. Table 1 shows the Gibbs free energy of the intermetallic phases from Ti-Al system [9, 10]. The $TiAl_3$ phase is formed first due to lower free enthalpy in comparison with $TiAl$ and Ti_3Al intermetallic phases. However, the $TiAl_2$ phase has the lowest Gibbs free energy. On the other hand, it forms only in the presence of the $TiAl$ as intermediate phase between $TiAl$ and Ti_3Al . S.E. Romanov

et.al. [11] observed the $TiAl_3$ phase in Ti-Al couple annealed at 600°C. However, they did not found diffraction lines of aluminum on the XRD diffraction pattern. This might be due to a thinner aluminum coating or the longer time of annealing. The XRD patterns obtained also show the decrease of intensity in diffraction lines of an aluminum in comparison with the sample annealed at 500°C.

TABLE 1
The Gibbs free energy of the intermetallic phases from the Ti-Al system [$J \cdot mol^{-1}$][9]

	500°C	600°C	700°C
Ti_3Al	-24448.3	-23777.5	-23106.7
$TiAl$	-24463.5	-22784.12	-21104.75
$TiAl_3$	-32337.3	-31300.77	-30264.23
$TiAl_2$	-35339.3	-34237.22	-33135.15
Ti_2Al_3	-33129.0	-32176.04	-31223.07

The XRD pattern of the sample annealed at 700°C reveal the presence of the Al, Ti, Al_3Ti , Ti_3Al and Al_2O_3 . The increase of intensity for $TiAl_3$ and decrease of intensity of diffraction peaks for aluminum is observed. The melting point of aluminum in vacuum is below 660°C. The presence of aluminum in the sample annealed at 700°C might be due to liquid phase reactions in aluminum TA6V-Al couple. It has been known that at the temperatures at about 700°C, Ti_3Al and $TiAl$ intermetallic phases are simultaneously formed at the Ti-Al interface and the $TiAl_3$ compound starts to decompose (Fig. 2) [11]. In the XRD diffraction pattern of the sample annealed at 700°C there were no diffraction lines of $TiAl$. The absence of this compound can be explained by early stages of the formation of $TiAl$ and Ti_3Al , which are confirmed by small volume fraction of the Ti_3Al phase in the sample annealed at 700°C (Table 2). Under the vacuum of 10^{-3} Pa the oxidation process at 700°C is not entirely excluded. As a result the Al_2O_3 compound was observed, which does not appear after annealing at lower temperatures.

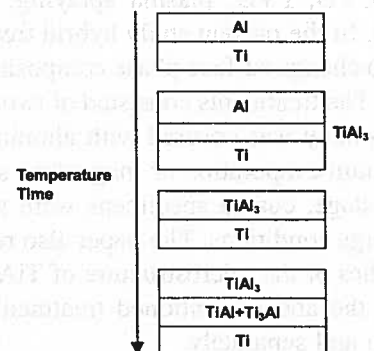


Fig. 2. Schematic explanations of the formation of aluminide phases

TABLE 2
The volume fractions of the compounds in TA6V-Al couple

Temp. [°C]	Ti [%]	Al [%]	TiAl ₃ [%]	Ti ₃ Al [%]	Al ₂ O ₃ [%]
500	39.7	60.3	—	—	—
600	34.2	59.4	6.4	—	—
700	37	1.9	48.9	10.7	1.5

Changes in the volume fraction of the compounds in TA6V-Al couple during the annealing are given in Table 2. It can be noted that the content of aluminum decreases and that of TiAl₃ rises with the increase of the annealing temperature (the volume fraction of Ti is constant). The Ti₃Al and TiAl compounds in the present study were observed only in sample annealed at 700°C.

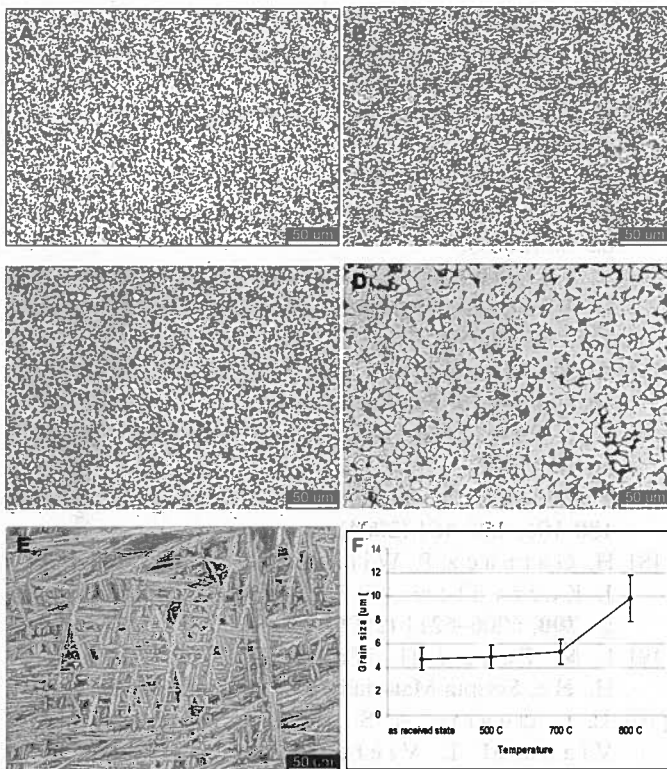


Fig. 3. The microstructure of the TA6V titanium alloy in the as received state (a) and after glow discharge annealing for 2 hour at: 500°C (b) 700°C (c) 800°C (d) 1000°C (e). Changes of the average grain size (equivalent diameter) of the α -Ti in as received state and after annealing at different temperatures are illustrated in (f)

Fig. 3 shows the microstructures of the TA6V titanium alloy in the as-received state and after annealing under glow discharge conditions at different temperatures. In the as-received state, the microstructure of the TA6V consisted of equiaxial grains of α -Ti and equilibrium volume fraction of β -Ti located at the “triple – points” of the α -Ti grains (Fig. 3a). The volume fraction of the α -Ti phase was 78% and the average grain size 4.7 μ m. Mechanical properties of the TA6V of such a microstructure are presented in Table 3.

TABLE 3
Mechanical properties of the TA6V titanium alloy used in the present work in as received state

Yield stress [MPa]	Tensile strength [MPa]	Elongation [%]	Microhardness [MPa]
995	1031	9.6	3300

The microstructures of the TA6V after glow discharge heat treatment at 500°C and 700°C for 2 hour (Fig. 3b,c) are comparable and similar to as-received state (Fig. 3a). In the sample annealed at 800°C the grains of α -Ti phase are significantly larger (Fig. 3.f). The microstructure of the samples subjected to glow discharge heat treatment at 1000°C changed from equiaxial type to plate like.

Influence of the surface treatments on the structure of the intermetallic layers

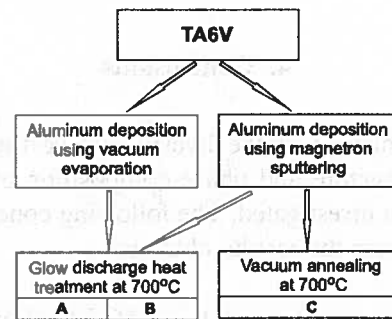


Fig. 4. Schematic explanation of the combinations of the hybrid engineering techniques employed in the present study

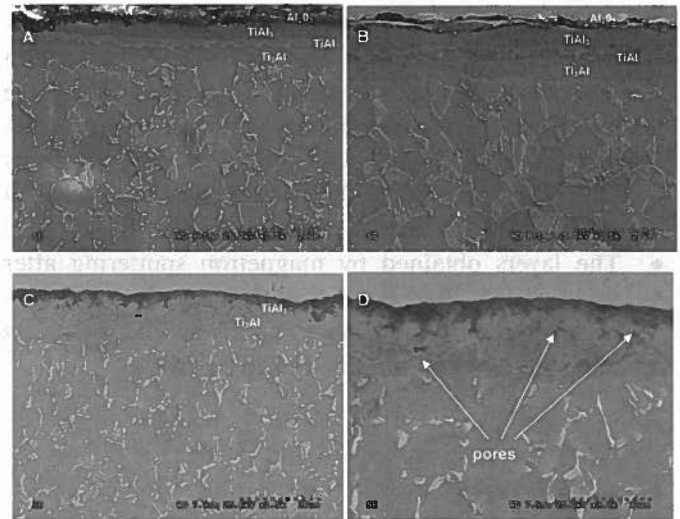


Fig. 5. The microstructures of the intermetallic layers obtained by: (a) vacuum evaporation and glow discharge heat treatment; (b) magnetron sputtering and glow discharge heat treatment; (c, d) magnetron sputtering and vacuum annealing. The image in (d) gives evidence to the high porosity of TiAl₃ layer

The hybrid surface techniques employed in this study are schematically presented in Fig. 4. Fig. 5 shows

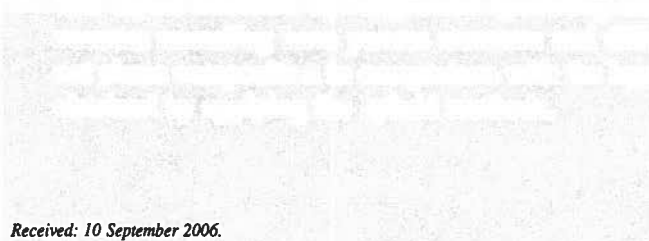
The mechanical properties of the TBM are shown in Table 1. The present work is concerned with

Property	Value
Young's Modulus (E)	210 GPa
Poisson's Ratio (ν)	0.3
Yield Stress (σ_y)	235 MPa
Tensile Strength (σ_t)	355 MPa
Compressive Strength (σ_c)	1000 MPa

Figure 1 shows the finite element mesh used for the analysis. The mesh is composed of 8-noded plane stress elements. The boundary conditions are shown in Figure 2. The applied loads are shown in Figure 3. The finite element analysis was performed using the ABAQUS finite element software.



Figure 1. Finite element mesh of the TBM.



Received: 10 September 2006.

The present work is concerned with the mechanical properties of the TBM. The present work is concerned with the mechanical properties of the TBM. The present work is concerned with the mechanical properties of the TBM.

The present work is concerned with the mechanical properties of the TBM. The present work is concerned with the mechanical properties of the TBM. The present work is concerned with the mechanical properties of the TBM.

The mechanical properties of the TBM are shown in Table 1. The present work is concerned with

Property	Value
Young's Modulus (E)	210 GPa
Poisson's Ratio (ν)	0.3
Yield Stress (σ_y)	235 MPa
Tensile Strength (σ_t)	355 MPa
Compressive Strength (σ_c)	1000 MPa

Figure 1 shows the finite element mesh used for the analysis. The mesh is composed of 8-noded plane stress elements. The boundary conditions are shown in Figure 2. The applied loads are shown in Figure 3. The finite element analysis was performed using the ABAQUS finite element software.

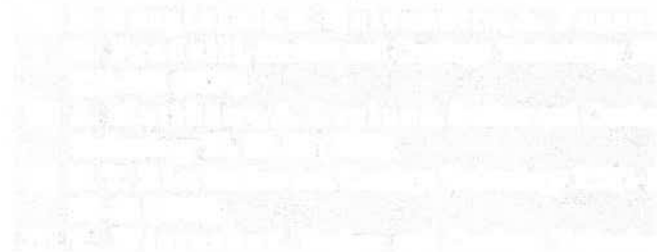


Figure 4. Finite element mesh of the TBM.

The present work is concerned with the mechanical properties of the TBM. The present work is concerned with the mechanical properties of the TBM. The present work is concerned with the mechanical properties of the TBM.